Astrophys Space Sci (2017) 362:208
DOI 10.1007/s10509-017-3190-0

ORIGINAL ARTICLE

A simple criterion for selecting disks with evidence for dust growth and settling

Yao Liu[1,2] · **Hongchi Wang**[1] · **Thomas Henning**[2]

Received: 3 July 2017 / Accepted: 9 October 2017 / Published online: 13 October 2017

Abstract Dust growth and settling, as an initial step of planet formation in protoplanetary disks, have an important impact on the appearance of the spectral energy distribution (SED). Selecting a promising sample of disks with signs of these processes helps to guide future observations towards a better understanding of the initial conditions for planet formation and disk evolution. Using a standard flared disk model, we conducted a large parameter study to investigate the effects of various disk parameters on the overall shape of the SED. We found that the flaring index and scale height can be used to mimic the effects of dust evolution on the SED. The influences of these two parameters on the infrared excess are very similar to that caused by dust evolution which have been shown in previous simulations where grain growth and settling are treated directly. Based on a statistic analysis of all the models in our grid, we proposed a criterion of $\Psi \geq 0.6$ to diagnose signs of dust evolution, where Ψ is a ratio defined by dividing a linearly interpolated (between 24 μm and 1.3 mm) flux at 70 μm by the observed 70 μm photometry. We tested the applicability of our criterion with the class II disks in the Taurus star formation region.

Keywords Circumstellar matter · Planetary systems: protoplanetary disks · Radiative transfer

✉ Y. Liu
yliu@pmo.ac.cn

[1] Purple Mountain Observatory & Key Laboratory for Radio Astronomy, Chinese Academy of Sciences, 2 West Beijing Road, Nanjing 210008, China

[2] Max Planck Institute for Astronomy, Königstuhl 17, 69117 Heidelberg, Germany

1 Introduction

Protoplanetary disks are a natural outcome of angular momentum conservation during the early phase of star formation, and play a fundamental role in the physical processes involved in star and planet formation. The dust and gas in the disk are the building blocks of planets. In the widely accepted core accretion model for planet formation (e.g., Lissauer and Stevenson 2007), dust grains coagulate and grow within the disks, settle towards the midplane driven mainly by the gravity of the central star, and are eventually assembled to larger entities, such as pebbles and planetesimals (e.g., Carballido et al. 2006; Dominik et al. 2007; Bitsch et al. 2015). Grain growth and settling are therefore considered as an initial step of planet formation process. Detailed analysis of a group of disks, which have signs of this crucial phenomenon, is the key to reveal the initial conditions for planet formation.

Analyzing the SEDs can yield evidences for dust growth in protoplanetary disks. A population of larger grains increases the emissivity at (sub)millimeter regime and makes the spectral index less steep than the micron-sized grains of the interstellar medium (e.g., Ricci et al. 2010; Testi et al. 2014; Pérez et al. 2015). Dust settling might be common in disks because observations show that most T Tauri stars have weaker mid-infrared fluxes than expected for a disk under the assumption of a well-mixed dust and gas phase (e.g., Furlan et al. 2005, 2006). The settling of dust towards the midplane leads to a reduced flaring angle of the disk and a decrease in infrared (IR) excess (e.g., D'Alessio et al. 2006). Mid-IR slopes are typically used as a probe for dust settling. Therefore, the SED contains abundant information about dust properties and disk geometry and can be used to identify promising targets for follow-up observations. As an example, through a detailed radiative transfer analysis, Liu

et al. (2012) found that an inclusion of grain growth and settling into the disk model is necessary to explain the weak far-IR excess observed in DoAr 33, a T Tauri star located in the Ophiuchus star formation region.

Nowadays, multi-wavelength survey conducted with the Spitzer (Evans et al. 2009), Herschel (André et al. 2010), JCMT (Ward-Thompson et al. 2007) and ALMA telescopes (e.g., Pascucci et al. 2016; Ansdell et al. 2016) have yielded a huge amount of data for the disks in the Gould Belt star formation regions. The booming observations result in a good sampling of the SED from IR to millimeter regime and offer an excellent opportunity to select a homogeneous sample of disks that have common features of early planet formation process. These pre-selected candidates are promising targets for future high-resolution observations that aim to reveal the initial conditions for planet formation. The ideal method to conduct the sample selection is a thorough radiative transfer modeling of the SED, see Liu et al. (2012) for a case study. However, the task becomes difficult when applying this strategy to a large number of objects because it is very computationally expensive. For instance, there are more than 200 young stellar objects in the Taurus star formation region (e.g., Rebull et al. 2010). It is very time-consuming to select the candidate disks with signs of dust evolution from them by individually fitting their SEDs under different model assumptions, e.g., whether or not dust settling is taken into account.

With a low degree of freedom, a standard flared disk model has been successfully used to explain multi-wavelength observations of protoplanetary disks such as the SED and high resolution images (e.g., Wolf et al. 2003; Andrews et al. 2011; Liu et al. 2015). In this model scenario, the flaring index and scale height are the two critical parameters characterizing the disk geometry, which in turn are expected to have a close link to the effects of dust growth and settling. In this work, using a flared disk model, we quantitatively investigate how these two parameters influence the overall shape of the SED via a large parameter study. Based on the results, we present a simple criterion for selecting candidate disks with evidence for dust evolution without the need for a full radiative transfer analysis of the SED. We test the applicability of the criterion using a large number of class II young stellar objects that have been identified in the Taurus star formation region.

2 Methodology

To investigate the effect of dust evolution on the overall shape of IR SED, one needs several steps. First, a parameterized model of a protoplanetary disk has to be introduced. Secondly, for all model parameters, we should decide whether they should be fixed to some typical value or vary within a certain range. The third step is to conduct the radiative transfer simulation for each model and analyze the result. We describe the first two steps in this section.

2.1 The model

We assume that dust and gas are well-mixed throughout the disk. The density structure of the dust is assumed to have a Gaussian vertical profile

$$\rho_{\rm dust} = \rho_0 R^{-\alpha} \exp\left[-\frac{1}{2}\left(\frac{z}{h(R)}\right)^2\right]. \quad (1)$$

The surface density distribution is parameterized with a power law

$$\Sigma(R) = \Sigma_0 R^{-p}, \quad (2)$$

where R is the distance from the central star measured in the disk midplane. Normalizing the total dust mass of the entire disk ($M_{\rm dust}$), one can determine the proportionality factors (ρ_0 and Σ_0) in Eqs. (1) and (2). The inner boundary of the density distribution is given by $R_{\rm in}$. We fix the disk outer radius ($R_{\rm out}$) to 200 AU, which is in agreement with typical sizes found for T Tauri disks (e.g., Andrews and Williams 2007). We do not explore this parameter in our study because it has negligible impact on the overall shape of the IR SED when the size of the disk is not extremely small. To allow flaring, the scale height $h(R)$ is described in a power-law form

$$h(R) = H_{100}\left(\frac{R}{100\ {\rm AU}}\right)^{\beta}, \quad (3)$$

where β is the flaring index characterizing the amount of flaring and H_{100} is a reference scale height at a distance of $R = 100$ AU.

2.2 Stellar heating

Protoplanetary disks can be heated by various mechanisms, for instance the accretion process and stellar irradiation. To reduce the degree of freedom, we only consider stellar irradiation as the heating source (e.g., Chiang and Goldreich 1997). We adopt a stellar luminosity of $L_\star = 1\ L_\odot$ and an effective temperature of $T_{\rm eff} = 4350$ K, representing the typical stellar properties of a T Tauri star. The stellar spectrum is taken from the Kurucz (1994) database for stellar model spectra, assuming $\log g = 3.5$ and solar metallicity.

2.3 Dust properties

The dust grains are assumed to be homogeneous spheres. We consider relative abundances of 62.5% silicate and 37.5%

graphite for the dust components. We take the refractive indices of "smoothed astronomical silicate" and graphite given by Weingartner and Draine (2001) to calculate the optical properties with Mie theory. For graphite, the extinction efficiency factor is computed by adopting the common "$\frac{1}{3} : \frac{2}{3}$" approximation (Draine and Malhotra 1993)

$$Q_{\rm ext,graphite} = \frac{1}{3} Q_{\rm ext}(\epsilon_{\parallel}) + \frac{2}{3} Q_{\rm ext}(\epsilon_{\perp}), \quad (4)$$

where $\epsilon_{\parallel}$ and $\epsilon_{\perp}$ are the components of the graphite's dielectric tensor for the electric field parallel and orthogonal to the crystallographic axis, respectively.

As the grain size distribution, we assume a power-law profile $n(a) \propto a^{-3.5}$ and a certain range for the size $a_{\rm min} \leq a \leq a_{\rm max}$. The commonly-known MRN distribution of the interstellar medium (ISM) has a minimum and maximum size of $a_{\rm min} = 5$ nm and $a_{\rm max} = 0.25$ μm, respectively (Mathis et al. 1977). We keep $a_{\rm min}$ fixed to 5 nm. The effect of dust growth in protoplanetary disks is simply simulated by increasing $a_{\rm max}$ to 1 mm (e.g., Ricci et al. 2010; Testi et al. 2014; Pérez et al. 2015).

2.4 The parameter space

As laid out above, we fixed the outer radius of the disk ($R_{\rm out}$), the stellar properties ($L_{\star}$ and $T_{\rm eff}$) and the grain size distribution ($a_{\rm min}$ and $a_{\rm max}$). Moreover, the disk inclination (i) is an external parameter. We took $i = 30°$ because it cannot be well constrained by SED analysis.

We allowed the disk inner radius ($R_{\rm in}$) to vary within a range of [1, 80 $R_{\rm sub}$], where $R_{\rm sub}$ is the sublimation radius of $R_{\rm sub} = 0.07\ (L_{\star}/L_{\odot})^{1/2}$, assuming a sublimation temperature of 1500 K for silicate (Dullemond et al. 2001). This is done in order to incorporate both the full disks without a central clearing of dust (Williams and Cieza 2011) and the transition disks in which large inner holes are present (e.g., Merín et al. 2010; Andrews et al. 2011; van der Marel et al. 2016). Given the stellar luminosity of 1 $L_{\odot}$, the lower and upper limits for the disk inner radius are 0.07 AU and 5.6 AU, respectively.

The flaring index β and scale height H_{100} are the two key parameters that determine the amount of IR excess emission. Previous modeling efforts have shown a variety of β and H_{100}. Good agreement between model and observations are found for values of $1.05 \leq \beta \leq 1.30$ and $5 \leq H_{100} \leq 20$ AU (e.g., Andrews et al. 2009, 2011; Olofsson et al. 2013; Liu et al. 2015). Therefore, we sampled them in a linear manner within these ranges.

The total dust mass spans a range of four orders of magnitude: $M_{\rm dust} = 5 \times 10^{-7}\ M_{\odot}$, $5 \times 10^{-6}\ M_{\odot}$, $5 \times 10^{-5}\ M_{\odot}$ and $5 \times 10^{-4}\ M_{\odot}$. The range is well consistent with the observed dust mass in disks that are located in nearby star formation regions (e.g., Andrews et al. 2013; Ansdell et al. 2016; Pascucci et al. 2016).

Table 1 Model parameters and their ranges explored in our study

Parameter	Fiducial model	Min	Max	Number of grid points
$T_{\star}$ [K]	4350	4350	4350	1
$L_{\star}$ [$L_{\odot}$]	1	1	1	1
$R_{\rm in}$ [$R_{\rm sub}$]	1	1	80	5
$R_{\rm out}$ [AU]	200	200	200	1
$M_{\rm dust}$ [$10^{-5} M_{\odot}$]	5	0.05	50	4
p	1.0	0.5	1.5	5
β	1.2	1.05	1.30	6
H_{100} [AU]	12.5	5	20	7
i [°]	30	30	30	1

We considered three values for the power-law index of the surface density profile: $p = 0.5$, 1.0 and 1.5. These are typical values obtained from previous modeling of a sample of disks (e.g., Andrews et al. 2009, 2010).

Table 1 summarizes the ranges and values for each parameter. In total, we have $5 \times 4 \times 5 \times 6 \times 7 = 4200$ different models in our grid.

3 Results

The radiative transfer problem is solved using the program `MC3D` (Wolf 2003) at 100 wavelengths, logarithmically distributed in the range of [0.5 μm, 4.0 mm]. As a result, a grid of 4200 model SEDs are prepared for investigating the impact of the model parameters, in particular the flaring index β and scale height H_{100}, on the overall shape of the SED.

3.1 The fiducial model

To discuss the result, we introduce a fiducial model. Its parameters are $R_{\rm in} = 1\ R_{\rm sub}$, $M_{\rm dust} = 5 \times 10^{-5}\ M_{\odot}$, $p = 1.0$, $\beta = 1.2$, $H_{100} = 12.5$ AU, see Table 1. This approach allows us to evaluate the impact of variations in the individual parameters on the SED. The blue lines in each panel of Fig. 1 show the SED of the fiducial model.

3.2 Effects of β and H_{100}

The total amount of IR excess emission highly depends on the temperature structure of the disk. In the radiative transfer model, the disk temperature is determined by how efficiently the dust intercepts and reprocesses the stellar energy. Most of that energy is absorbed by dust grains in the disk's photosphere, where the visible optical depth is around unity, i.e., $\tau_{0.55\ \mu\rm m} \sim 1$. Dust grains in a large surface area of a flared disk can be directly illuminated by the central star. The flaring index β is used to control the vertical extent of the disk

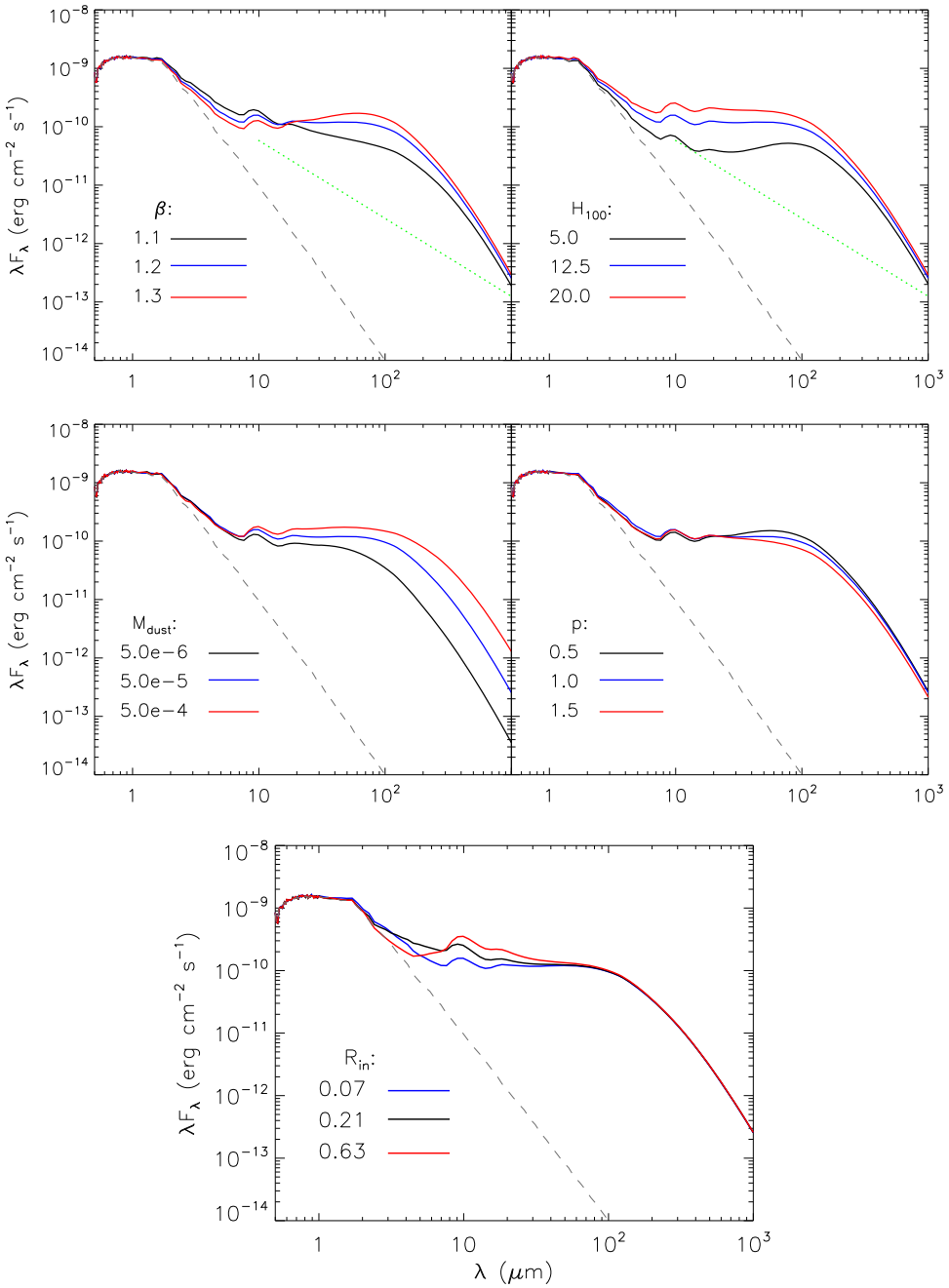

Fig. 1 SED visualization showing the impact of disk parameters on the IR emission, i.e., flaring index β and scale height H_{100} (*upper panel*), total dust mass $M_{\rm dust}$ and surface density index p (*middle panel*) and inner disk radius $R_{\rm in}$ (*bottom panel*). The *green dotted lines* correspond to the spectral slope of $-4/3$ for a perfectly flat disk (Dullemond et al. 2007). Parameters not listed in each plot are identical to those of the fiducial model, see Table 1. The *blue lines* refer to the fiducial model, whereas the *grey dashed lines* symbolize the contribution of the central star to the total flux

at each radius, and therefore it determines how the intercepted stellar energy is stored into disk surface layers as a function of radius. Higher flared disks (with a larger β) will re-emit more of that energy from larger radii, where the temperature is relatively cooler. Since cooler dust preferentially emits at longer wavelengths, a larger β will produce more far-IR emission.

Similarly, vertically extended (larger H_{100}) disks are heated more efficiently and have higher temperatures. Therefore, a larger scale height generates brighter emission at mid-IR wavelengths. Figure 1 (upper panel) shows the impact of β and H_{100} on the IR SED. In order to have a direct view of their implications, we only vary one particular parameter in each plot, while other parameters are set to the fiducial values. It can be seen that disks with larger β or H_{100} feature more IR excess.

3.3 Effects of $M_{\rm dust}$, p and $R_{\rm in}$

The flux intensity is proportional to the total amount of dust material. Hence, it is straightforward to understand that lower dust masses produce less thermal emission. The parameter p governs how steep the power-law surface density

profile is. A shallower index makes more dust concentrated in the outer region of the disk where the temperature is relatively cool, and consequently re-emits more far-IR flux. The disk inner radius $R_{\rm in}$ sets up the location at which dust grains start to distribute inside-out. The IR excess is a result of dust thermal emission. In our model, we assume there is no dust inside the region $R < R_{\rm in}$, i.e., there is a central empty cavity with a size of $2R_{\rm in}$. Therefore, the inner boundary of the disk is a pivotal parameter to establish the maximum dust temperature, which in turn shapes the near-IR SED and determines the wavelength at which the excess emission becomes prominent.

Figure 1 (middle and bottom panels) shows the impact of these three parameters on the SED. It is clear that the flux density at IR to millimeter regime scales with the total dust mass $M_{\rm dust}$, the surface density index p has a mild influence on the far-IR emission and the shape of near-IR SED is significantly affected by the disk inner radius $R_{\rm in}$.

3.4 Comparison with previous parametric studies

Woitke et al. (2016) proposed a set of assumptions for the modeling of protoplanetary disks, which consists of continuum radiative transfer, thermo-chemical modeling of gas and line radiative transfer. They systematically investigated the effects of those assumptions on the various continuum (including the SED) and line predictions in a parametric way. The effects of β, H_{100}, $M_{\rm dust}$, p and $R_{\rm in}$ on the SED shown in Fig. 8 in their paper are well consistent with our results, although the assumed dust properties and surface density profile are different between both works. Similar trends are also seen for disks in a lower stellar mass regime, see Fig. 10 in Bulger et al. (2014).

3.5 Link disk geometry parameters to dust evolution

Dust grains in protoplanetary disks experience a gravitational force by the central star. They gradually settle toward the disk midplane. In the meanwhile, grain growth accelerates this process because larger grains have a shorter time scale of being settled. As a result, (sub)micron-sized grains are present in the surface layers of the disk while large (e.g., millimeter-sized) dust grains tend to concentrate close to the midplane. Dullemond and Dominik (2004) analyzed how the process of dust settling affects the SED using radiative transfer models that take both the settling and vertical turbulent stirring into account. Their results show that small grains quickly settle down to a scale height that is often well below the original location of the disk's photosphere. The optical appearance of the disk becomes effectively "flatter", since the small grains are the main contributor to the opacity. As the system evolves, the depletion of small dust grains in the disk surface layers leads to depressed mid- to far-IR emission, see Fig. 5 and Fig. 7 in Dullemond and Dominik (2004).

D'Alessio et al. (2006) presented self-consistent disk models of T Tauri stars that include a parameterized treatment of dust settling and grain growth. In their prescription, dust settling is modeled by using two grain size distributions: a small grain population and a large grain population. The small grains are distributed in the upper layers while the disk interior (i.e., close to the midplane) is filled with large dust grains, see Sect. 4.3. A parameter ϵ is used to describe the depletion factor of the small grains in the upper layers, i.e., mimicking the degree of dust settling. Their results show that the height of the irradiation surface decreases with ϵ, reducing the stellar energy intercepted by the disk and consequently the far-IR excess.

In our simulation, we do not iterate the vertical structure of the disk under an assumption of hydrostatic equilibrium. The geometric thickness of the disk as a function of radius in our models is fully parameterized by β and H_{100}, see Eq. (3). This approach has an advantage that different geometry structures (i.e., different combinations of β and H_{100}) can be explored in a flexible way. Therefore, it is naturally understood that we observe a similar trend of the IR excess on β or H_{100} to the modeling results in which dust evolution is directly included. A consequence of dust evolution is to lower either (or both) of these two parameters, and plays an important role to shape the IR SED.

3.6 Criterion for diagnosing dust evolution

In the upper panel of Fig. 1, we draw the flux prediction of a perfectly flat disk, see green dotted lines. It is characterized by a power law with a slope of $-4/3$ (Dullemond et al. 2007) and can be considered as an extreme case for significant dust settling. We introduce a ratio Ψ to simply diagnose the evidence for dust evolution. More specifically, this ratio is derived by dividing the linearly interpolated flux at 70 μm by the model 70 μm flux. The interpolation is performed by using the data at 24 μm and 1.3 mm. The upper diagram of Fig. 2 gives a sketch and the ratio is described via $\Psi = F_{\rm linear.70}/F_{\rm model.70}$.

In general, Ψ increases as the settling proceeds until it approaches to 1, which is the value for the perfectly flat disk. We chose 24 μm as the lower limit of the wavelength for the interpolation because the effect of settling on the SED starts to be prominent at this point, see Fig. 1. For the upper boundary, we used 1.3 mm (i.e., not any shorter wavelength) due to the fact that millimeter photometry is a good probe for the total dust mass since the disk becomes optically thin at this wavelength regime. Including millimeter measurements into the analysis highly reduces the possibility of a low dust mass being the cause of weak IR excess, see the middle left plot of Fig. 1.

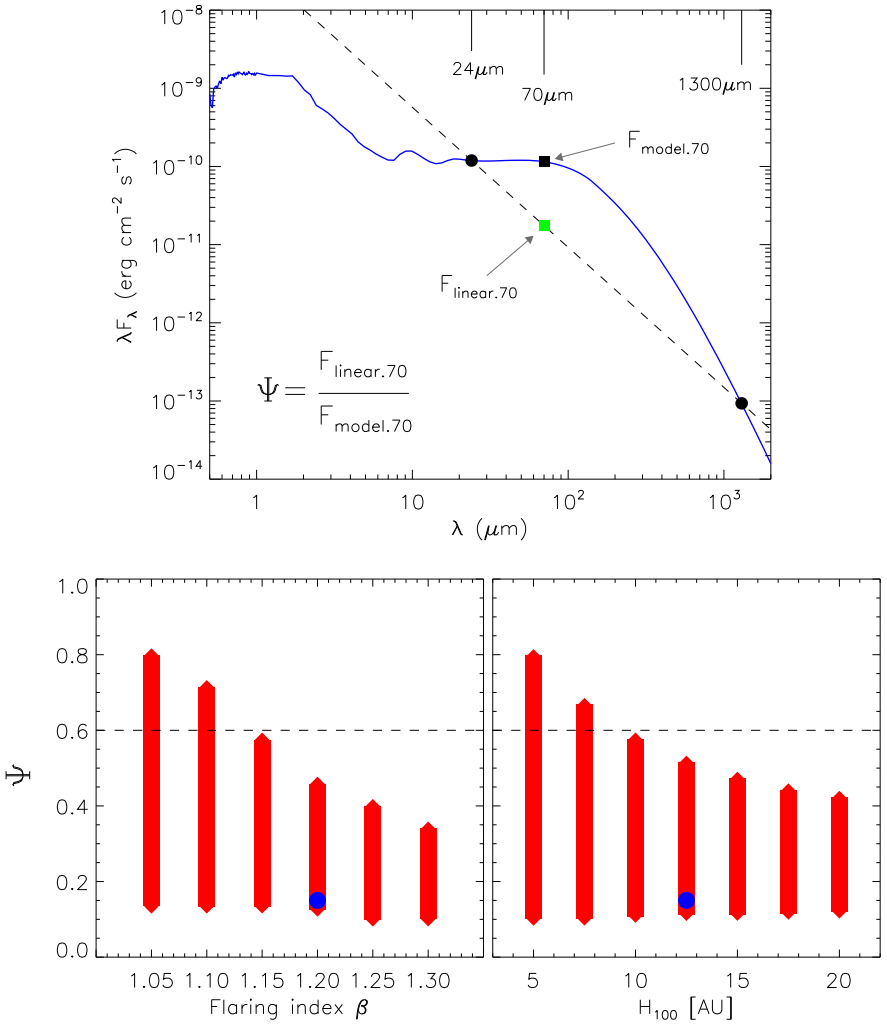

Fig. 2 *Upper panel*: An illustration of the criterion used to select disks with evidence for dust evolution. The *blue solid line* shows the SED of the fiducial model. The *green square* refers to a linear interpolation at 70 μm ($F_{\rm linear.70}$) using model fluxes at 24 μm and 1.3 mm as highlighted with *black dots*. The model flux at 70 μm ($F_{\rm model.70}$) is shown as a *black square*. The ratio is defined as $\Psi = F_{\rm linear.70}/F_{\rm model.70}$. *Lower panel*: The range of Ψ as a function of H_{100} and β obtained from analyzing all the models in our grid. The *blue dots* mark the position of the fiducial model. The *horizontal lines* shows $\Psi = 0.6$, which is the suggested value used to select the promising candidates

We calculated Ψ for all the 4200 models in the grid and derived its range as a function of β or H_{100}. The result is shown in the lower panel of Fig. 2. It is clear to see that the maximum value of Ψ in each bin increases with decreasing β or H_{100}, i.e., with dust settling, supporting the idea that Ψ can be used as a diagnosis of dust evolution. As indicated in Table 1, the model grid is a result of different combinations of all the parameters. For instance, there are models with a small β but with a very large H_{100}, and vice versa. So we also have small Ψs with little flaring or with a thin disk. The horizontal dashed lines refer to $\Psi = 0.6$, which is for the T Tauri star DoAr 33. In Liu et al. (2012), we conducted a detailed SED modeling for this object. We found that if dust and gas are well-mixed (i.e., no dust settling), models with β and H_{100} as low as $\beta \sim 1.05$ and $H_{100} \sim 5.5$ AU still overpredict the far-IR flux, which is strong evidence for dust evolution in its disk. Therefore, we believe that $\Psi = 0.6$ is a good threshold to determine whether the effect of dust settling on the appearance of the SED becomes significant. This is also a value that can be achieved only by models with small flaring indices or scale heights, see the lower panel of Fig. 2.

3.7 Gap formation as the dominant reason for weak far-IR excess?

Meeus et al. (2001) introduced a classification scheme of Herbig Ae/Be stars based on the shape of the mid- to far-IR continuum. A source was classified as "group II" when the continuum follows a power-law profile and "group I" when an additional cold component is present on the top of the power-law continuum. These two categories were originally thought to represent a difference in disk morphology. Group I sources have flared disks while the disk around group II sources is flat or self-shadowed. From an evolutionary point of view, group II sources were proposed to be an evolved version of group I sources due to dust coagulation, growth and settlement (e.g., Dullemond and Dominik 2004).

Our understanding of disk evolution, in particular for Herbig Ae/Be disks, is rapidly changing. Recent high-resolution imaging shows that many group I sources have

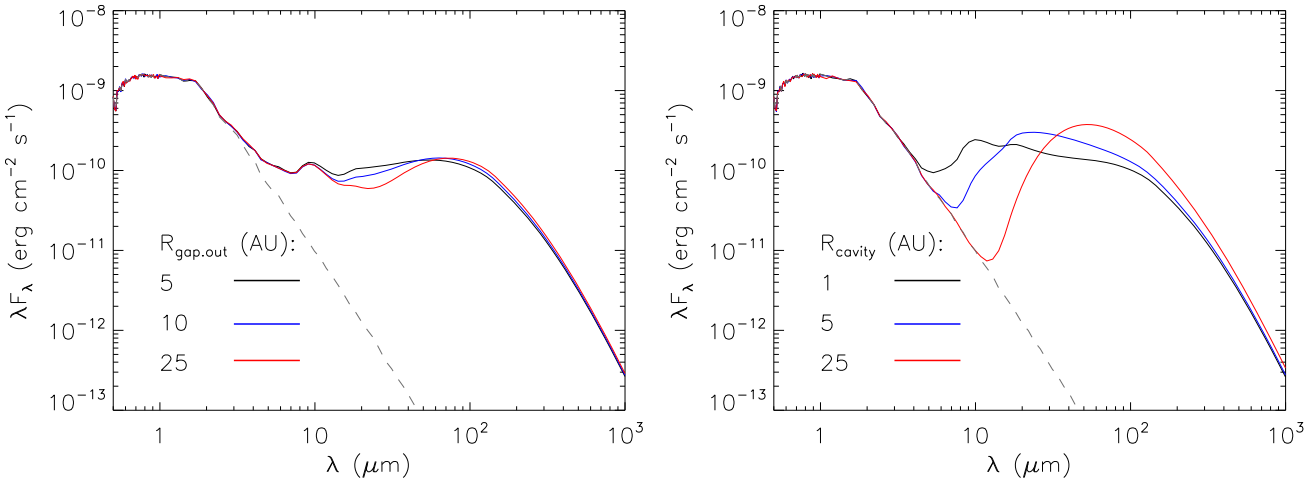

Fig. 3 SED visualization showing the impact of gap or cavity opening on the IR SED. For the gapped disk (*left panel*), the configuration consists of an inner disk ($0.07 \leq R \leq 1$ AU), a gap (1 AU $< R <$ $R_{\rm gap.out}$) and an outer disk ($R \geq R_{\rm gap.out}$). For the cavity scenario (*right panel*), there is a central hole with a radius of $R_{\rm cavity}$ in the disk. Other parameters not listed in the plot, such as β, H_{100} and $M_{\rm dust}$, are identical to the fiducial values

a disk with large (tens of AU) gaps or cavities while group II disks are gapless (e.g., Maaskant et al. 2013; Menu et al. 2015; Garufi et al. 2017). As a result, Maaskant et al. (2013) suggested a new evolutionary scenario in which group I and group II sources are different successors of a common ancestor: a primordial flared disk. The two groups represent different pathways in the evolution of disks. Gap formation has proceeded the collapse of the outer disk in group I sources whereas dust growth and settling drive the evolution of the outer disk into a flat geometry in group II sources.

The direct consequence of gap opening is to remove dust grains inside the gap, which in turn reduces the excess emission at a wavelength range depending on the size and location of the gap. Therefore, whether gap formation can be the dominant mechanism for the diminished far-IR (in particular at 70 μm) excess should be discussed, although there is probably a trend that in general group II disks have lower far-IR flux than group I sources, see Fig. 5 in Garufi et al. (2017).

We investigated the effects of gap (or cavity) opening on the far-IR SED with a small parameter study. The result is shown in Fig. 3. The left panel refers to the gapped disk, where the configuration consists of an inner disk ($0.07 \leq R \leq 1$ AU), a gap ($1 < R < R_{\rm gap.out}$) and an outer disk ($R \geq R_{\rm gap.out}$). For the cavity scenario which we show in the right panel, the disk has a central hole with a radius of $R_{\rm cavity}$. We explored $R_{\rm gap.out}$ and $R_{\rm cavity}$ and found that their effects on the SED are pronounced at near- and mid-IR wavelengths. This suggests that gap (or cavity) opening may be a less important factor to influence the far-IR excess compared to the role of dust growth and settling for T Tauri disks. On one hand, disks are born in different flavors in terms of size, mass, host stellar properties and etc. On the other hand, gap (or cavity) opening and dust settling are more likely to work together during the evolution of disks. Therefore, a thorough parameter study based on a more realistic model is required to clarify the issue, which is beyond the scope of this paper.

4 Application of the criterion

Based on a grid of radiative transfer models, we have investigated the effect of dust evolution on the overall shape of IR SED and proposed a simple criterion for selecting candidate disks with evidence for dust evolution. In this section, we apply the criterion to real targets and test its applicability.

4.1 The Taurus molecular cloud

As illustrated in Fig. 2, the criterion requires the object being detected at 24 μm, 70 μm and 1.3 mm simultaneously. These photometry can be obtained by observations with the Spitzer/MIPS, Herschel/PACS instruments and radio telescopes. The Taurus molecular cloud is a nearby (∼140 pc), young (1–2 Myr) star formation region with a low stellar density (Reipurth 2008). Previous deep and wide coverage surveys via various programs, such as the Taurus Spitzer Survey (Padgett et al. 2008), have identified a robust and effectively complete sample of class II disks (e.g., Rebull et al. 2010). With the unprecedented capacity, the Herschel space telescope brings a huge amount of far-IR data for Taurus, which cannot be accessible before (Howard et al. 2013; Bulger et al. 2014). These new observations together with the (sub-)millimeter census of young stellar objects (YSOs) in Taurus (e.g., Beckwith et al. 1990; Andrews et al. 2013)

Table 2 Target properties

The data except for Ψ are directly taken from Andrews et al. (2013). The stellar masses are derived by interpolating the pre-main-sequence evolutionary tracks given in Siess et al. (2000)

Object name	RA (J2000)	DEC (J2000)	SpT	$T_{\rm eff}$ (K)	$L_\star$ ($L_\odot$)	$M_\star$ ($M_\odot$)	$A_{\rm v}$ (mag)	Ψ
BP Tau	04:19:15.8	+29:06:26.9	K7	4050	0.97	0.79	0.75	0.75
FZ Tau	04:32:31.7	+24:20:03.0	M0	3850	1.26	0.45	3.81	0.65
IRAS 04370+2559	04:40:08.0	+26:05:25.3	K6–M3.5	3778	0.90	0.32	10.65	0.93
J04155799+2746175	04:15:57.9	+27:46:17.5	M5.5	3058	0.08	0.10	1.38	1.0

make Taurus an ideal place to test the criterion in a sample scale.

4.2 Taurus disks with evidence for dust evolution

Andrews et al. (2013) have built a catalog of 178 class II disks that have a good wavelength coverage of data from optical to millimeter regime. A complete SED atlas of these objects can be found in appendix A of their paper. We analyzed this sample and found 4 disks with $\Psi \geq 0.6$. There are two considerations in the analysis. First, we preferred to use the Herschel/PACS 70 μm photometry when both the Spitzer/MIPS and Herschel/PACS data at 70 μm are available, because the latter has a higher sensitivity. Secondly, the diverse set of literature millimeter flux measurements needs to be homogenized. For objects without photometry at the "reference" wavelength (i.e., $\lambda = 1.3$ mm), we used the available data at $\lambda > 1.3$ mm to generate a representative flux density from an extrapolation to the "reference" wavelength. The extrapolation was done from a power-law fit, where $F_\nu \propto \nu^\alpha$ with $\alpha = 2.4$ (Andrews et al. 2013). The properties of the 4 candidates, for instance the stellar temperature and luminosity, are listed in Table 2.

4.3 Full radiative transfer modeling of the SEDs

We performed thorough SED modeling for the four disks in order to check whether dust evolution is indeed required to explain the data. A well-mixed disk model that is described in Sect. 2.1 was first used to reproduce the observed SEDs. This model has a parameter space of $\{R_{\rm in}, M_{\rm dust}, \alpha, \beta, H_{100}\}$.

Then, we introduced a settled disk model to take the effect of dust evolution into account. Detailed assumptions for this kind of model can be found in Liu et al. (2012). Here, we briefly describe the setup. We used two dust populations, i.e., a small dust population ($a_{\rm max} = 0.25$ μm) and a large dust population ($a_{\rm max} = 1$ mm). The large dust grains are distributed at a lower scale height (i.e., closer to the disk midplane) than that of the small grain population:

$$h_{\rm small} = H_{100}\left(\frac{R}{100\ {\rm AU}}\right)^\beta \tag{5}$$

$$h_{\rm large} = h_{\rm small}/H_{\rm ratio}. \tag{6}$$

The dust-to-gas mass ratios are assumed different between the two grain populations. This is to mimic grain growth and settling by moving mass from the small grain population to the midplane. A parameter

$$\epsilon = \frac{\zeta_{\rm small}}{\zeta_{\rm ISM}} \tag{7}$$

is used to quantify the depletion degree of the small dust grains relative to the standard dust-to-gas ratio of the ISM (D'Alessio et al. 2006), where $\zeta_{\rm ISM} = 0.01$ and $\zeta_{\rm small}$ is the dust-to-gas mass ratio in the small dust grain population. The settled disk model has a parameter space of $\{R_{\rm in}, M_{\rm dust}, \alpha, \beta, H_{100}, H_{\rm ratio}, \epsilon\}$.

Simulated annealing (SA), a versatile optimization technique based on the Metropolis-Hastings algorithm, was invoked to search for the best fit (Kirkpatrick et al. 1983). Details about the implementation of SA for SED modeling are given in the appendix of Liu et al. (2012). The disk inclination was fixed to 30° within the fitting loop because a constraint on this parameter is mostly from spatially resolved observations. The best fit models are shown in Fig. 4, whereas Table 3 lists the corresponding parameter sets. For convenience, we designate the well-mixed and settled disk models with a uppercase "W" and "S", respectively. The full radiative transfer analysis indicates that the well-mixed model overpredicts the far-IR photometry for all the targets while an inclusion of dust evolution into the modeling highly improves the interpretation of the data. This feature is similar to what we found for DoAr 33 and directly demonstrates the applicability of our simple criterion proposed for selecting disks with evidence for dust evolution. These promising candidates deserve follow-up observations, especially high-resolution imaging at (sub)millimeter wavelengths, to unveil their structure and evolutionary stage.

5 Summary

Dust growth and settling are considered as the first step towards planet formation in protoplanetary disks. Detailed analysis of a homogeneous sample of disks, which have signs of dust evolution, is the key to reveal the initial conditions for planet formation and understand how the formation of planets relates to disk evolution. Selecting a large

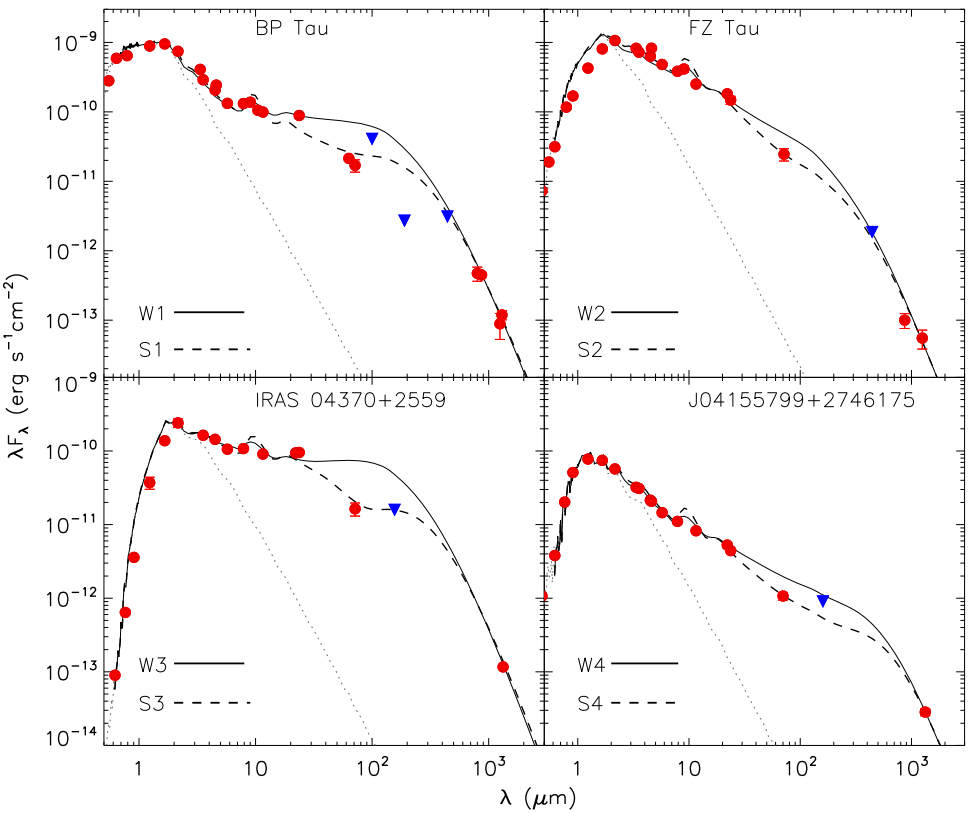

Fig. 4 Best-fit models of the 4 Taurus disks using the well-mixed (W1, W2, W3, W4; *solid lines*) and settled disk model (S1, S2, S3, S4; *dashed lines*). The *red dots* depict the photometric measurements whereas the *blue triangles* represent a upper limit of flux density. The *gray dotted lines* mark the contribution of the central star to the total flux of the system. *Error bars* for the photometry are shown if they are larger than the symbol. Flux densities at different wavelengths are from Andrews et al. (2013), Howard et al. (2013), Bulger et al. (2014) and references therein

Table 3 The parameter sets of the SED models shown in Fig. 4

Parameter	Model							
	W1	S1	W2	S2	W3	S3	W4	S4
$R_{\rm in}$ [AU]	0.07	0.08	0.20	0.18	0.21	0.21	0.02	0.02
$M_{\rm dust}$ [10^{-5} $M_\odot$]	7.00	10.0	3.00	4.2	10.0	17.5	10.0	15.0
α	2.15	2.14	2.05	2.06	2.20	2.09	2.05	2.06
β	1.15	1.16	1.05	1.04	1.20	1.18	1.05	1.06
H_{100} [AU]	15.0	20.5	12.5	12.6	10.0	10.2	12.5	13.5
$H_{\rm ratio}$	1.0	2.5	1.0	2.4	1.0	5.3	1.0	1.9
ϵ	1.0	0.19	1.0	0.74	1.0	0.37	1.0	0.45
i [°]	30	30	30	30	30	30	30	30

sample of disks with evidence for dust evolution helps to guide future observations, but it is a computationally expensive task since it requires a full radiative transfer modeling of the available observations, e.g., the SED.

Dust growth and settling can flatten or attenuate the disk, which alters the optical appearance of the disk and in turn influences the IR excess emission. Using a flared disk model, we conducted a large parameter study to investigate these effects. We found that the disk geometry parameters (i.e., flaring index and scale height) can be used to mimic the effect of dust evolution on the SED in an indirect but simple way. Varying these two parameters has a similar impact on the IR SED as compared to the simulation results in which dust evolution is directly taken into account. Dust thermal emission at IR in particular far-IR wavelengths decreases with low flaring indices or scale heights. Based on a statistic analysis of all the models in our grid, we introduced a ratio Ψ to diagnose the signs of dust evolution. The ratio is defined by dividing a linearly interpolated flux at 70 μm by the observed 70 μm photometry. The interpolation makes use of the data at 24 μm and 1.3 mm. We selected four promising candidates from 178 Taurus class II disks with a criterion of $\Psi \geq 0.6$. A thorough SED modeling for these four targets demonstrates the applicability of the criterion. Our simple criterion has a clear advantage that it does not require a full radiative transfer analysis of the SED, which benefits large sample studies a lot.

Acknowledgements Y.L. acknowledges supports by the Natural Science Foundation of Jiangsu Province of China (Grant No. BK20141046) and by the NSFC grant 11503087.

References

André, P., Men'shchikov, A., Bontemps, S., et al.: Astron. Astrophys. **518**, L102 (2010)
Andrews, S.M., Williams, J.P.: Astrophys. J. **659**, 705 (2007)
Andrews, S.M., Wilner, D.J., Hughes, A.M., Qi, C., Dullemond, C.P.: Astrophys. J. **700**, 1502 (2009)
Andrews, S.M., Wilner, D.J., Hughes, A.M., Qi, C., Dullemond, C.P.: Astrophys. J. **723**, 1241 (2010)
Andrews, S.M., Wilner, D.J., Espaillat, C., et al.: Astrophys. J. **732**, 42 (2011)
Andrews, S.M., Rosenfeld, K.A., Kraus, A.L., Wilner, D.J.: Astrophys. J. **771**, 129 (2013)
Ansdell, M., Williams, J.P., van der Marel, N., et al.: Astrophys. J. **828**, 46 (2016)
Beckwith, S.V.W., Sargent, A.I., Chini, R.S., Guesten, R.: Astron. J. **99**, 924 (1990)
Bitsch, B., Lambrechts, M., Johansen, A.: Astron. Astrophys. **582**, A112 (2015)
Bulger, J., Patience, J., Ward-Duong, K., et al.: Astron. Astrophys. **570**, A29 (2014)
Carballido, A., Fromang, S., Papaloizou, J.: Mon. Not. R. Astron. Soc. **373**, 1633 (2006)
Chiang, E.I., Goldreich, P.: Astrophys. J. **490**, 368 (1997)
D'Alessio, P., Calvet, N., Hartmann, L., Franco-Hernández, R., Servín, H.: Astrophys. J. **638**, 314 (2006)
Dominik, C., Blum, J., Cuzzi, J.N., Wurm, G.: Protostars and Planets V, p. 783 (2007)
Draine, B.T., Malhotra, S.: Astrophys. J. **414**, 632 (1993)
Dullemond, C.P., Dominik, C.: Astron. Astrophys. **421**, 1075 (2004)
Dullemond, C.P., Dominik, C., Natta, A.: Astrophys. J. **560**, 957 (2001)
Dullemond, C.P., Hollenbach, D., Kamp, I., D'Alessio, P.: Protostars and Planets V, p. 555 (2007)
Evans, N.J. II, Dunham, M.M., Jørgensen, J.K., et al.: Astrophys. J. Suppl. Ser. **181**, 321 (2009)
Furlan, E., Calvet, N., D'Alessio, P., et al.: Astrophys. J. **628**, L65 (2005)
Furlan, E., Hartmann, L., Calvet, N., et al.: Astrophys. J. Suppl. Ser. **165**, 568 (2006)
Garufi, A., Meeus, G., Benisty, M., et al.: Astron. Astrophys. **603**, A21 (2017)
Howard, C.D., Sandell, G., Vacca, W.D., et al.: Astrophys. J. **776**, 21 (2013)
Kirkpatrick, S., Gelatt, C.D., Vecchi, M.P.: Science **220**, 671 (1983)
Kurucz, R.: Solar Abundance Model Atmospheres for 0, 1.2, 4.8 km/s, p. 19. Smithsonian Astrophysical Observatory, Cambridge (1994). Kurucz CD-ROM No. 19
Lissauer, J.J., Stevenson, D.J.: Protostars and Planets V, p. 591 (2007)
Liu, Y., Madlener, D., Wolf, S., Wang, H., Ruge, J.P.: Astron. Astrophys. **546**, A7 (2012)
Liu, Y., Joergens, V., Bayo, A., Nielbock, M., Wang, H.: Astron. Astrophys. **582**, A22 (2015)
Maaskant, K.M., Honda, M., Waters, L.B.F.M., et al.: Astron. Astrophys. **555**, A64 (2013)
Mathis, J.S., Rumpl, W., Nordsieck, K.H.: Astrophys. J. **217**, 425 (1977)
Meeus, G., Waters, L.B.F.M., Bouwman, J., et al.: Astron. Astrophys. **365**, 476 (2001)
Menu, J., van Boekel, R., Henning, T., et al.: Astron. Astrophys. **581**, A107 (2015)
Merín, B., Brown, J.M., Oliveira, I., et al.: Astrophys. J. **718**, 1200 (2010)
Olofsson, J., Szűcs, L., Henning, T., et al.: Astron. Astrophys. **560**, A100 (2013)
Padgett, D.L., Rebull, L.M., McCabe, C., et al.: Taurus Spitzer Legacy Project Data Release 2: Catalog and Mosaics for the Entire Survey (2008). Available from: http://irsa.ipac.caltech.edu/data/SPITZER/Taurus/docs/delivery_doc2.pdf
Pascucci, I., Testi, L., Herczeg, G.J., et al.: Astrophys. J. **831**, 125 (2016)
Pérez, L.M., Chandler, C.J., Isella, A., et al.: Astrophys. J. **813**, 41 (2015)
Rebull, L.M., Padgett, D.L., McCabe, C.-E., et al.: Astrophys. J. Suppl. Ser. **186**, 259 (2010)
Reipurth, B.: Handbook of Star Forming Regions, Volume I: The Northern Sky (2008)
Ricci, L., Testi, L., Natta, A., Brooks, K.J.: Astron. Astrophys. **521**, A66 (2010)
Siess, L., Dufour, E., Forestini, M.: Astron. Astrophys. **358**, 593 (2000)
Testi, L., Birnstiel, T., Ricci, L., et al.: Protostars and Planets VI, p. 339 (2014)
van der Marel, N., Verhaar, B.W., van Terwisga, S., et al.: Astron. Astrophys. **592**, A126 (2016)
Ward-Thompson, D., Di Francesco, J., Hatchell, J., et al.: Publ. Astron. Soc. Pac. **119**, 855 (2007)
Weingartner, J.C., Draine, B.T.: Astrophys. J. **548**, 296 (2001)
Williams, J.P., Cieza, L.A.: Annu. Rev. Astron. Astrophys. **49**, 67 (2011)
Woitke, P., Min, M., Pinte, C., et al.: Astron. Astrophys. **586**, A103 (2016)
Wolf, S.: Comput. Phys. Commun. **150**, 99 (2003)
Wolf, S., Padgett, D.L., Stapelfeldt, K.R.: Astrophys. J. **588**, 373 (2003)